Deon, F., Koch-Müller, M., Rhede, D., Wirth, R. (2010): Water and Iron effect on the P-T-x coordinates of the 410-km discontinuity in the Earth upper mantle. - Contributions to Mineralogy and Petrology, 161, 4, 653-666

DOI: 10.1007/s00410-010-0555-6

Fiorenza Deon, Monika Koch-Müller, Dieter Rhede and Richard Wirth

Water and Iron effect on the P-T-x coordinates of the 410-km discontinuity in the Earth upper mantle

Helmholtz Zentrum Potsdam, Deutsches GeoForschungsZentrum-GFZ
Telegrafenberg, 14473 Potsdam, Germany.
Corresponding author: Fiorenza Deon
fdeon@gfz-potsdam.de
Tel.: +49-331-2881887
Fax: +49-331-2881402

Abstract

We performed multi-anvil experiments in the system MgO-SiO_2 ± H_2O at 13.0-13.7 GPa and 1,025-1,300°C and in the system MgO-FeO-SiO_2 ± H_2O, under reducing conditions, at 11.0-12.7 GPa and 1200°C, to depict the effect of H_2O on the P-T-x coordinates of the 410-km discontinuity, i.e. the olivine-wadsleyite phase boundary. The charges were investigated with Electron Microprobe (EMP), Raman Spectroscopy, Fourier Transform Infrared Spectroscopy (FTIR), Secondary Ion Mass Spectrometry (SIMS) and Electron Energy Loss Spectroscopy (EELS). We observe in the MgO-SiO_2-H_2O system at 1,200°C a 0.6 GPa shift of the phase boundary to lower pressure compared to dry conditions, due to the stronger water fractionation into wadsleyite (wad) rather than in olivine (ol). In the MgO-FeO-SiO_2-H_2O system we reproduced the triple point, i.e. observed coexisting hydrous ol, wad and ringwoodite (ring). SIMS H quantifications provided partitioning coefficients for water: $D^{water}_{wad/ol}$ ~ 3.7(5) and $D^{water}_{ring/ol}$ ~ 1.5(2) and $D^{water}_{wad/ring}$ ~ 2.5(5). For a bulk composition of x_{Fe} = 0.1 our data indicate only a slight difference in the width of the loop of the two phase field ol-wad under hydrous conditions compared to dry conditions, i.e. no broadening in respect to composition but a shift to lower pressures. For bulk compositions of $x_{Fe} > 0.2$, i.e. in regions where wad-ring and ol-ring coexist, we observe, however, an unexpected broadening of the loops with a shift to higher iron contents. In total the stability field of hydrous wad expands in both directions, to lower and higher pressures. Fe^{3+} concentrations as determined by EELS are very low and are expected to play no role in the broadening of the loops.

Keywords: Earth upper mantle, 410-km discontinuity, ol-wad phase transition, high pressure, water quantification.

Introduction

It is now generally accepted that the 410- and 660-km discontinuities in the Earth's mantle are related to an important change in the mantle density of 5 and 10%, respectively, which causes discontinuous changes in the P and S seismic wave velocities (e.g. Dziewonski and Anderson 1981).

The seismic 410-km discontinuity is related to the phase transformation of olivine α-$(Mg,Fe)_2SiO_4$ (ol) into its high P polymorph wadsleyite β–$(Mg,Fe)_2SiO_4$ (wad) (e.g. Ringwood, 1975, Katsura and Ito, 1989). Both minerals belong to the category of NAMs (Nominally Anhydrous Minerals), which may incorporate hydrogen[1] in the form of hydroxyl in their structure. Experimental studies (e.g. Kohlstedt et al.1996; Smyth 2006; Mosenfelder et al. 2006) demonstrated that ol, the most abundant constituent of the Earth's upper mantle, may incorporate up to 0.9 wt % H_2O. Its high P polymorphs wad and ring (γ-$(Mg,Fe)_2SiO_4$) are also known to act as water reservoir: wad can incorporate in its structure as much as 3 wt% H_2O as calculated by Smyth (1987) and later experimentally shown by Inoue et al. (1995) and ring may store up to 2.8 wt % H_2O (e.g. Kohlstedt et al. 1996). As Keppler and Bolfan Casanova (2006) showed, the difference in water contents is strictly related to the P-T conditions and phase assemblies.

Water is carried down into the mantle via subduction of oceanic plates, and usually most of it is released at depth of 150 km; however, experiments and seismic observations imply that hydrogen can be transported much deeper, it is even discussed that it occurs as light element in the Earth's core. Previous seismic tomographic observation evidence that the 410-km discontinuity is in some region of the Earth upper mantle quite sharp, i. e. 6 km, (Yamazaki et al. 1994, Rost et al. 2002) but much broader in other regions as shown by van der Meijde et al. (2003): under the Mediterranean, the broadness varies between 20 and 30 km. This may be linked to variable water concentrations. In other words, the water distribution in the Earth

[1] Further on expressed either with wt ppm H_2O or with the general term "water"

upper mantle, may be inhomogeneous, due to the history of subduction and amount of water incorporated by the phases characterizing these depths. Wood (1995) investigated the effect of water on the region where ol and wad coexist theoretically and proposed a shift of 0.6 GPa to lower P and broadening of 22 Km of the 410-km discontinuity by assuming 500 wt ppm H_2O in ol and 5,000 wt ppm H_2O in wad.

The influence of water on the position and shape of the ol-wad phase transition, i.e. on the 410-km discontinuity, is still a highly discussed issue and experimental studies do show contradictory results (Chen et al. 2002; Frost and Dolejs 2007). Chen et al. (2002) observed basically no difference between anhydrous and hydrous conditions in the Mg_2SiO_4 end-member system at 12.6-14.7 GPa and 1200°C, but the experiments performed by Frost and Dolejs show a shift of 1 GPa to lower pressures under the same conditions when water is included in the system. In the system $(Mg_{0.91}\text{-}Fe_{0.09})_2SiO_4$ Chen et al. (2002) detected a shift toward lower iron contents and a decrease of the pressure width of the ol-wad loop to 0.3 GPa under water saturated conditions compared to dry conditions for experiments at 12.6-14.4 GPa and 1,200°C.

A further important parameter which may influence the P-T-x coordinates is the Fe^{3+} content. In a recent study Frost and McCammon (2009) showed that in oxidizing conditions very strong partitioning of Fe^{3+} into wad shifts both phase boundaries of the ol-wad loop to lower Fe-contents.

In this study we focus on the role of water on the ol-wad phase boundary in the $MgO\text{-}SiO_2\text{-}H_2O$ and the $MgO\text{-}FeO\text{-}SiO_2\text{-}H_2O$ systems by performing experiments under reducing conditions. Thus, the aim of this study is to clarify the effect of water on the P, T, x coordinates of the ol-wad phase transition.

Experimental methods

Multi-anvil syntheses

Experiments were performed in a multi-anvil apparatus similar to that of Walker (1991) but with a special tool that allows alternatively a continuous 360° rotation or a 180° rocking motion of the Walker high-pressure module during the run with 5° per sec in order to avoid separation of the fluid from the solid parts of the run and thus ensure a homogenous starting material (see Schmidt and Ulmer 2004). This was applied to all hydrous runs but one (MA192). A 14/8-mm assembly (octahedron length/truncation length) was used for each experiment, consisting of a MgO-based octahedral pressure medium with a stepped graphite heater, MgO and/or BN spacers and pyrophyllite gaskets. Dry experiments in the system $MgO\text{-}SiO_2$ are -among others- the base of the P calibration of the multi-anvil experiments where the α–β transition curve of the study of Morishima et al. (1994) has been taken as reference (13.6 GPa -1,200°C). In some experiments, the pressure was calculated using the $(Mg,Fe)_2SiO_4$ phase relations (see Frost and Dolejs, 2007). Details of the experimental set up are given in Deon et al. (2009).

Table 1a and 1b list the experimental conditions and starting materials. The chemical compounds were mixed and homogenized for 15 min before being placed in a 3-mm-long platinum capsule with a diameter of 2 mm. As starting material for the hydrous runs, a stoichiometric Mg_2SiO_4 oxide-hydroxide mixture $(MgO + SiO_2)$-$Mg(OH)_2$ was used, yielding to a H_2O-content of the bulk of 5 wt %. To buffer the SiO_2 activity, we added 5 wt% $MgSiO_3$ enstatite to the starting material. The $Mg(OH)_2$ (brucite) was synthesized in a hydrothermal cold sealed apparatus at 0.4 GPa and 700°C from MgO plus water in excess. We verified the presence of excess water at the end of each hydrous experiment by placing the recovered and opened Pt capsule in an oven at 170°C and checking the weight difference before and after heat treatment. The dry runs were performed with synthetic forsterite and wad seeds as starting material without rotation/rocking of the press.

For the experiments in the system $MgO\text{-}FeO\text{-}SiO_2$, we chose two sets of bulk initial compositions: $(Mg_{1.8}Fe_{0.2})SiO_4$ and $(Mg_{1.85}Fe_{0.15})SiO_4$. For the set of hydrous experiments in

Table 1a. List of experimental constraints and of the electron microprobe (EMP) analysis of the experiments in the system $MgO\text{-}SiO_2 \pm H_2O$.

Experiment	P (GPa) (±0.3)	*T* (°C) (±25)	Starting material[a, b]	Duration (hrs.)	Product+en	EMPA: c.p.f.u (cation per formula unit)
MA063 calib.	13.4	1,025	Forsterite Mg_2SiO_4	24	wad	
FD062 Calib.	13.3	1,025	Forsterite Mg_2SiO_4	7	wad	
FD063 calib.	13.3	1,100	Forsterite Mg_2SiO_4	7	wad	
FD0727 calib.	13.4	1,100	Forsterite[c]	6	wad	
FD0826 calib.	13.3	1,200	Forsterite	5	ol	
FD0831 calib.	13.7	1,200	Forsterite	6	wad	
FD0836	13.3	1,150	$MgO\text{-}SiO_2$ $Mg(OH)_2$	6	wad-phase E	$Mg_{(1.92)}Si_{(1.04)}O_4$
MA207	13.2	1,150	$MgO\text{-}SiO_2$ 6 μL H_2O	8	wad	
FD0715	13.0	1,200	$MgO\text{-}SiO_2$ $Mg(OH)_2$	5	wad-fo-phase E	
FD0718	13.3	1,200	$MgO\text{-}SiO_2$ $Mg(OH)_2$	6	wad	$Mg_{(1.92)}Si_{(1.04)}O_4$
FD0723	13.2	1,250-1,300[d]	$MgO\text{-}SiO_2$ $Mg(OH)_2$	6	ol	Mg_2SiO_4
FD0713	13.3	1,300	$MgO\text{-}SiO_2$ $Mg(OH)_2$	6	wad	

[a]The following chemical were used: MgO, FeO (99.9% pure) Iron Oxide II Aldrich; SiO_2 (99.999%) pure Alpha Aesar.
[b]In all the starting materials, except in the calibration (calib.) experiments, 5 wt% $MgSiO_3$ was added.
[c] Synthesized from a gel in annealing experiments.
[d] Due to the failure in the thermocouple the final temperature is estimated from the power reading as 1,250-1,300°C.

Table 1b: List of experimental constraints and of the Electron microprobe (EMP) analyses of the experiments in the system $MgO\text{-}FeO\text{-}SiO_2 \pm H_2O$

Experiment	P GPa (±0.3)	T°C (±25)	Starting material[a,b]	Duration (hrs.)	Product+en	EMPA (c.p.f.u)	#Fe=Fe/(Fe+Mg)	$K_{wad/ol}^{Fe/Mg} = \left[\frac{(Fe/Mg)_{wad}}{(Fe/Mg)_{ol}}\right]$
FD0832	12.2	1,200	$(Mg_{1.8}Fe_{0.2})SiO_4$ (oxide mixture)	30	ol-wad	ol:$Mg_{1.89}Fe_{0.2}Si_{0.97}O_4$ wad:$Mg_{1.55}Fe_{0.47}Si_{0.99}O_4$	ol:0.12(1) wad:0.23(1)	wad/ol=2.86
FD0839	12.4	1,200	$(Mg_{1.8}Fe_{0.2})SiO_4$ (oxide mixture)	30	ol-wad	ol:$Mg_{1.83}Fe_{0.22}Si_{0.97}O_4$ wad:$Mg_{1.58}Fe_{0.41}SiO_4$	ol:0.11(1) wad:0.21(1)	wad/ol=2.15
FD0843	12.4	1,200	$(Mg_{1.85}Fe_{0.15})SiO_4$	30	ol-wad-maj	ol:$Mg_{1.88}Fe_{0.18}SiO_4$ wad:$Mg_{1.54}Fe_{0.46}SiO_4$ maj:$Mg_{2.8}(Fe_{0.72}Al_{1.41}Si_{0.17})(SiO_4)_3$	ol:0.09(1) wad:0.23(3) maj:0.22(2)	wad/ol=3.12
FD0848	12.0	1,200	$(Mg_{1.8}Fe_{0.2})SiO_4$ (oxide mixture)	29	ol-wad	ol:$Mg_{1.73}Fe_{0.23}SiO_4$ wad:$Mg_{1.41}Fe_{0.52}SiO_4$	ol:0.14(1) wad:0.27(2)	wad/ol=2.77
MA192 static	12.2	1,200	$(Mg_{1.8}Fe_{0.2})SiO_4$ 1.7 µL H_2O	30	ol-wad-ring	ol:$Mg_{1.71}Fe_{0.33}SiO_4$ wad:$Mg_{1.41}Fe_{0.61}SiO_4$ ring:$Mg_{1.16}Fe_{0.87}SiO_4$	ol:0.16 (1) wad:0.30(4) ring:0.43(1)	wad/ol=2.24 wad/ring=0.58 ring/ol=3.88
FD0833	12.2	1,200	$(Mg_{1.8}Fe_{0.2})SiO_2$ 1.7 µL H_2O	30	ol-wad-ring	ol:$Mg_{1.76}Fe_{0.29}Si_{0.97}O_4$ wad:$Mg_{1.47}Fe_{0.54}SiO_4$ ring:$Mg_{1.2}Fe_{0.8}Si_{0.99}O_4$	ol:0.14(1) wad:0.27(1) ring:0.41(1)	wad/ol=2.23 wad/ring=0.55 ring/ol=4.86

Experiment	P GPa (±0.3)	T°C (±25)	Starting material	Duration (hrs.)	Product+en	EMPA (c.p.f.u.)	#Fe=Fe/(Fe+Mg)	$K_{wad/ol}^{Fe/Mg} = \left[\frac{(Fe/Mg)_{wad}}{(Fe/Mg)_{ol}}\right]$
FD0844	12.7	1,200	$(Mg_{1.85}Fe_{0.15})SiO_4$ 0.40 µL H_2O	30	ol-wad-maj	ol: $Mg_{1.87}Fe_{0.16}SiO_4$ wad: $Mg_{1.66}Fe_{0.37}SiO_4$ maj:$Mg_{2.81}(Fe_{0.71}Al_{1.46}Si_{0.14})(SiO_4)$	ol:0.08(1) wad:0.18(2) maj:0.20(3)	wad/ol=2.60
FD0849	12.0	1,200	$(Mg_{1.80}Fe_{0.20})SiO_4$ 0.35 µL H_2O	30	ol-wad	ol:$Mg_{1.82}Fe_{0.19}SiO_4$ wad:$Mg_{1.59}Fe_{0.39}SiO_4$	ol:0.10(1) wad:0.20(1)	wad/ol=2.34
FD0853	11.0	1,200	$(Mg_{1.6}Fe_{0.4})SiO_4$ 0.4 µL H_2O	29	ol-ring	ol:$Mg_{1.59}Fe_{0.42}SiO_4$ ring:$Mg_{0.86}Fe_{1.13}SiO_4$	ol:0.21(2) ring:0.57(1)	ring/ol=4.85

[a]The following chemicals were used: MgO, FeO (99.9%) Iron oxide II Adrich; SiO_2 (99.999% pure) Alpha Aesar.
[b]In all starting materials 5 wt% $MgSiO_3$ was added

the MgO-FeO-SiO_2-H_2O system, three initial starting materials were used: $(Mg_{1.7}Fe_{0.3})SiO_4$, $(Mg_{1.8}Fe_{0.2})SiO_4$ and $(Mg_{1.85}Fe_{0.15})SiO_4$ prepared from oxide mixtures and/or olivine solid solutions. In the hydrous multi-anvil experiments, distilled water was added, and in all experiments, the recovered capsule had still water in excess, as the weight difference proves. To keep the fO_2 low, we placed metallic Fe wrapped in a perforated Pt-foil at the bottom of the Pt capsule.

The ol solid solutions were synthesized in a high –T gas mixing furnace under reducing atmosphere in 30 hrs. Oxygen fugacity (fO_2) was obtained with CO_2-H_2 (Ar) gases mixtures and monitored by zirconia-based solid electrolyte oxide sensor from Ceramic Oxide Fabricators ^{TM}. The furnace was placed around a vertical 110-cm-long corundum tube with 50 mm inner diameter, where the central part of the tube was uniformly heated. The gas mixture was introduced at the top of the furnace tube and allowed the gas mixture to exit at the bottom. The temperature, 1300°C during the experiments, was controlled by a thermocouple and stabilized by an electronic device with a total variation less than 0.5°C. The output of the temperature and oxygen fugacity was controlled with a sensor without interruption during the experiments and stored in a computer. The fO_2 in the syntheses was chosen between the magnetite wüstite and the wüstite iron buffer.

In two experiments, the starting material was accidentally impured with corundum from our experimental set up, as we observed the occurrence of the Al-bearing phase majorite (see results).

Electron Microprobe

Almost all the capsules were cut vertically in two halves: one half was embedded in epoxy resin in a glass mount with the minimum quantity of epoxy needed. Only in one case, (FD0718), the capsule was emptied and single crystals were embedded in epoxy. After polishing, the composition of the samples were determined by EMP. Point analyses and element distribution mapping (Mg, Fe, Si) were carried out at the GFZ using a JEOL thermal

field emission type electron-probe JXA-8500F (HYPERPROBE). The analytical conditions included an accelerating voltage of, 15 kV, a beam current of 10 nA and a focused beam (< 40 nm diameter) Standards were a well-characterized synthetic forsterite (Mg_2SiO_4) and Fe_2O_3. Peak counting times were 20 s, and the backgrounds were counted for 10 s. The raw intensity data were corrected with the Armstrong-CITZAF on-line correction program (Armstrong, 1995).

Secondary Ion Mass Spectrometry

The ^{1}H content of the Fe-bearing ol, wad and ring was measured by Secondary Ion Mass Spectrometry (SIMS) using a CAMECA ims 6f ion probe at the GFZ. Before each session, the instrument was baked for at least 48 hours. The vacuum was enhanced by using liquid nitrogen via a permanent filling liquid nitrogen Dewar, which ensured that the total vacuum pressure in the sample chamber during the analysis was always better than 4E-08 Pa. The samples were prepared as described in the EMPA section. For SIMS measurement, the samples were cleaned in an ultrasonic bath with pure ethanol, stored at 70 °C before being covered with an approximately 30 nm high pure gold and were put into the airlock chamber (12 positions) to outgas at a pressure better than 3E-07 Pa for more than 3 days. A primary $^{16}O^-$ beam was accelerated to 12.5 kV; the beam current was set to 2 nA and focused to about 10 µm diameter on the sample surface. Prior to each spot analysis, a 40 µm X 40 µm area was presputtered of 120 s to reduce the surface contamination. Positive secondary ions were extracted using a potential of 10 kV and the energy window was placed at a width equal to 50 eV. A mass resolving power of $M/\Delta M = 3{,}000$ was used which is sufficient to resolve ^{30}Si from the nearby $^{29}Si^{1}H$ interferences. Counting times per cycle were 15 s for ^{1}H and 2 s for ^{30}Si. The average acquisition time was 70 min, and the $^{1}H/^{30}Si$ ratios were calculated by averaging only the last 100 cycles from each analysis.

To build a calibration curve, the $^{1}H/^{30}Si$ ratios of 4 reference samples were calibrated against the H_2O/SiO_2 (wt ppm/wt %) ratio from the reference materials to determine the water content

(Fig.1).

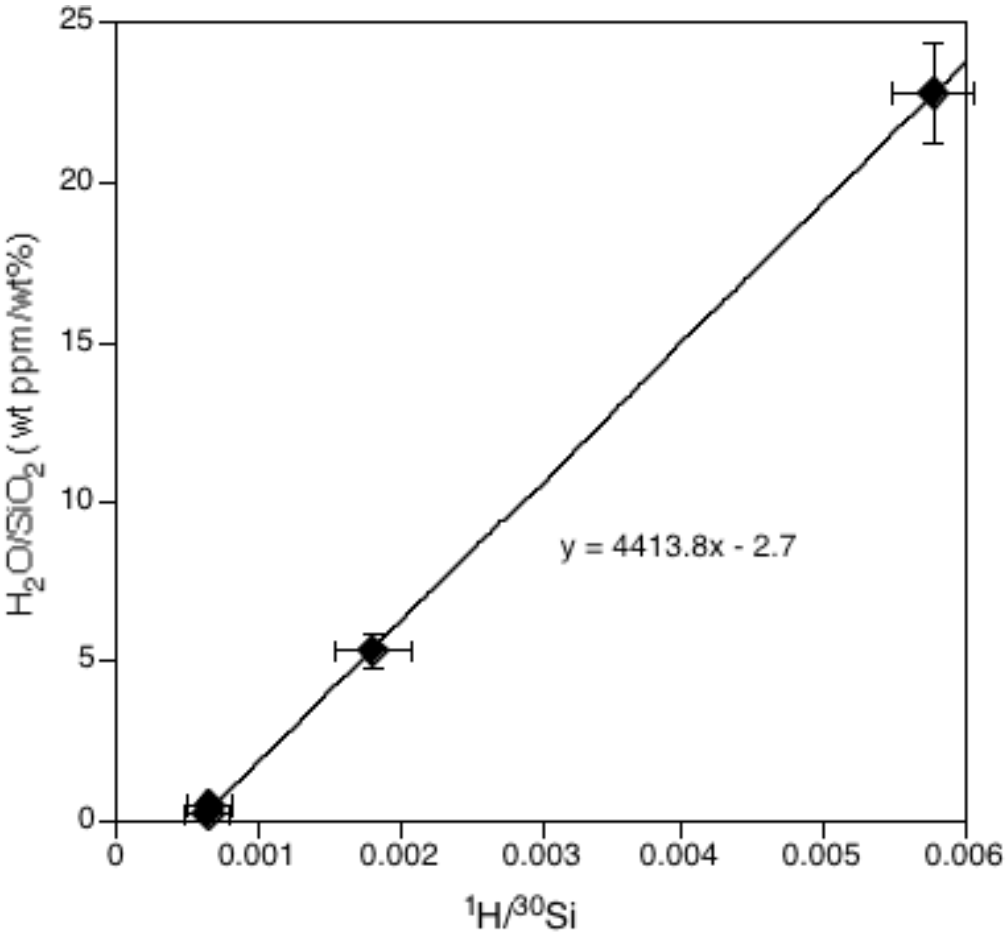

Fig. 1

Figure 1 SIMS calibration curve for water, showing $^{1}H/^{30}Si$ vs. H_2O/SiO_2 (wt ppm/wt%) for the garnets and olivine. Each data point is an average of more than 5 single measurements with the corresponding error bars. Regression parameters for the SIMS calibration curve are indicated in the plot.

Three well-characterized garnets (870 wt ppm H_2O, 207 wt ppm H_2O, 18 wt ppm H_2O) (Maldener et al. 2003, Thomas et al. 2008) and a synthetic olivine (8 wt ppm H_2O) were used as reference materials, whose water contents were measured with independent techniques.

With this calibration curve and standards used, we could well reproduce the water concentration in synthetic hydrous Mg-wad (sample FD0718) whose concentration was also independently determined by Raman spectroscopy as 8500(1000) wt ppm (Deon et al. 2009).

Raman spectroscopy

The spectra were collected in the range of 200-1,200 $cm^{-1}$for 20 s on all samples for phase identification. One sample (FD0833) was measured in the range 3,000-3,800 cm^{-1} to obtain a water quantification to compare with the SIMS measurements.

The spectra measured in this study were all acquired with a Horiba-Jobin Yvon Labram HR 800 UV-VIS spectrometer (grating 1800 grooves/mm) in a backscattering configuration using a CCD detector (1024 elements), an Argon Laser and an Olympus optical microscope with a long working distance 100x objective (LWD VIS, NA = 0.80, WD = 3.4 mm). For sample excitation, we used the 488 nm Ar^+ line and a laser power of 300 mW. The confocal pinhole of 100 μm was used, which corresponds to a spectral resolution of about 1 cm^{-1}.

For water quantification, we applied the Comparator technique (Thomas et al. 2008 and 2009). Unpolarized spectra in the spectral range between 3,000 – 3,800 cm^{-1} were measured directly on wad crystals of experiment FD0833, which were analyzed before using SIMS and EMP. Although the sample contained Fe, no correction to account for the absorption of the initial and scatter laser light was necessary (see optical spectra in Ross 1997). The laser beam was first focused on the sample surface using a 100x objective, then lowered 4 μm to avoid errors due to surface inhomogeneities of the crystal. A spectrum of the reference glass bearing 8.06 wt % water was recorded in the beginning and at the end of each measuring time. Spectra acquisition time was 100 s, with 3 accumulations for the sample, and 20 sec and 3 accumulations for the

reference. All the spectra were normalized using this reference. A linear background correction in the spectral range between 3,170 – 3,750 cm^{-1} was carried out on each spectrum.

FTIR spectroscopy

Unpolarized IR spectra were measured on hydrous Fe-bearing crystals: wad (FD0849), ol and ring (both FD0853) using a Bruker IFS66v FTIR spectrometer connected to a Hyperion microscope. We used a Globar as light source, a KBr beam, splitter and an InSb detector. The spectra were collected with a resolution of 2 cm^{-1} and averaged over 256 accumulated scans in the OH stretching region between 2,500 cm^{-1} and 4,000 cm^{-1}. The aperture size was chosen between 30 x 30 and 80 x 80 μm according to the dimension of the crystals. The water content was calculated averaging 5 unpolarized spectra for wad of the charge FD0849 and 5 unpolarized spectra for each ol and ring from charge FD0853 using the Beer-Lambert relation $c_{H2O} = A_{i,tot} \times 1.8/(t \times \rho \times \varepsilon)$ where c is the water concentration (wt %), $A_{i,tot}$ is the mean value of the total integrated intensities (cm^{-1}) deriving from the fit of the FTIR unpolarized spectra and multiplied by 3 (corresponding to the orientation factor introduced by Paterson (1982) which considers the three crystallographic directions as the spectra are unpolarized), t the thickness of the crystals (cm) and ρ the densities. For hydrous minerals and glasses ε–values can be taken from the general calibrations published by, e.g. Paterson (1982), or Libowitzky and Rossman (1997). However, it has been shown that these values should not be applied to water quantification in nominally anhydrous minerals (NAMs); NAMs need mineral-specific ε–values (e.g. Rossman 2006, Thomas et al. 2009, Koch-Müller and Rhede, 2010). Therefore, absorption coefficients (ε) were taken from Deon et al. (2009) for wad, 73,000 ± 7,000 L mol H_2O cm^{-2}, from Koch-Müller et al. (2006), 37,500 ± 5,000 L mol H_2O cm^{-2}, and Koch-Müller and Rhede (2010) 75,300± 7,000 L mol H_2O cm^{-2} for ol and ring, respectively. Unpolarized IR spectra in the OH stretching region were also collected on some crystals of anhydrous runs to check whether they are really dry. All spectra collected throughout this study were fitted with

the program PeakFit by Jandel Scientific (version 4.11) using the 2nd derivative zero algorithm for the background and a mixed Gaussian and Lorenzian distribution function for the component bands. The algorithm for the background fitting is unique to PeakFit and was applied in the spectral range 2,500-4,000 cm^{-1}. The algorithm is based on the fact that baseline points tend to exist where the second derivative of the data is both constant and zero.

Transmission Electron Microscopy

For TEM investigations, site-specific foils were cut by the Focused Ion Beam technique (FIB) directly from the embedded capsules. The instrument used was a FEI FIB200 with Ga-ion source operating at 30 kV. Details of FIB TEM sample preparation are given elsewhere (Wirth, 2004). TEM was performed using a FEI Tecnai$^{TM}G^2$ F20 X-Twin transmission electron microscope equipped with a Gatan imaging filter (GIF) and an EDAX-X-ray spectrometer. Energy-filtered lattice fringe images, electron energy loss spectra (EELS) and the chemical composition of the samples were obtained on all phases of the FD0833 experiment. EELS (Electron Energy Loss Spectroscopy) spectra were acquired with a collection angle 2β of 12 mrad and an illumination angle of 2α of 4 mrad. The EELS aperture was 2 mm, and the energy dispersion 0.1 eV/pixel, to avoid an alteration in the oxidation state the acquisition time was 1 s. The energy resolution of the filter was 0.9 eV at half width at full maximum of the zero loss peak. Spectra were acquired in diffraction mode with an acquisition time of 1 s in order to avoid oxidation of the iron. Lauterbach et al. (2000) applied 10 - 30 s integration time; however, their samples were cooled to nearly liquid nitrogen temperature. As a test of our experimental setup, we determined the Fe^{3+} concentration for a spinelloid (sample MA27) with 32 % of its Fe as Fe^{3+} (Koch-Müller et al. 2009). The Fe^{3+} content of each phase of the FD0833 sample was calculated averaging 5 EEL spectra collected on the same FIB foil from slightly different locations and following the method described by Van Aken et al. (1998). Two 2 eV wide integrating windows were applied to the $L_{2,3}$-peaks: from

708.5 to 710.5 eV for the L_3-edge for Fe^{3+} and from 719.7 to 721.7 eV for the L_2-edge for Fe^{2+}. We were not able to perform Mössbauer spectroscopic measurements to quantify Fe^{3+} because we did not obtain a sufficient quantity of crystals to apply this method.

Results

Syntheses

Run products were identified with X-ray diffraction, Raman and FTIR spectroscopy and are all listed in Table 1a, for the system MgO-SiO_2±H_2O, and in Table 1b for the system MgO-FeO-SiO_2 ± H_2O. Figure 2 show cross-sections through different experimental charges. In Fig. 2a the capsule of the hydrous experiment FD0723 in the system MgO-SiO_2-H_2O is shown as a Si distribution map. The major occurring phase can be distinguished from the Si-richer enstatite and the Mg-Si enriched quenched fluid. Although en was added roughly to the starting material, it always occurs along the capsule walls. We believe this to be related to the Soret diffusion during the heating process, which lasts approximately 30 min. The thermal gradient during the heating (colder capsule core compared to the walls) causes a gradient in the chemical potential, which results in Si enrichments in the hotter capsule walls compared to the capsule core (see Schmidt and Ulmer, 2004). Experiments in the system MgO-SiO_2-H_2O results either in wad or ol. As ol and wad do contain different amounts of water there should be a range where both coexist. However, this range is hard to be experimentally reproduced due to the sharpness of the phase transition and our small temperature gradient with the capsule.

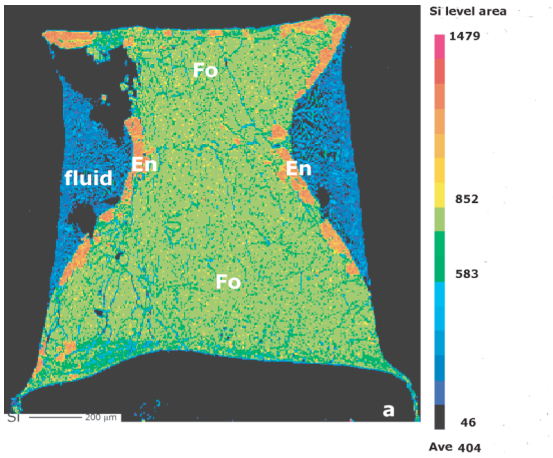

Fig. 2a

Figure 2a) Si distribution mapping from the electron microprobe showing a cross-section of a multi-anvil Pt capsule from the hydrous experiment FD0723: the green area (Mg richer) shows ol; the orange spots prove the presence of en and the blue part on both sides are referred to the fluid. The intensity color scale represents the distribution of Si in the section.

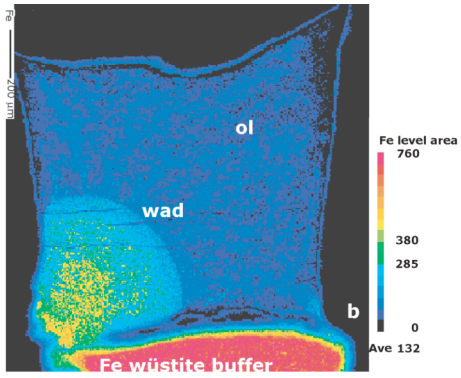

Fig. 2b

Figure 2b) Fe-distribution mapping from the electron microprobe showing a cross-section of a multi-anvil Pt capsule of anhydrous experiment FD0832: two main occurring phases can be observed, i.e. a lighter blue (Fe richer) wad and a darker blue (Mg richer) ol. In the lower part of the section, the red area (highest Fe content) represents the Fe-wüstite buffer. The intensity color scale represents the distribution of Fe in the section.

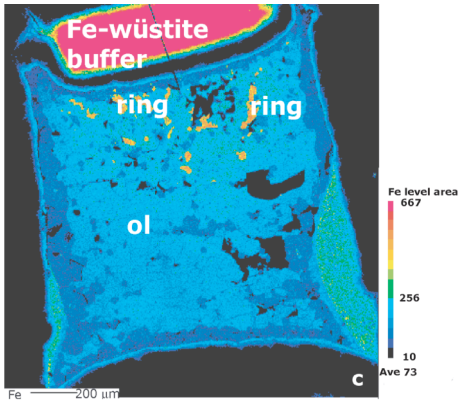

Fig. 2c

Figure 2c) Fe-distribution mapping from the electron microprobe showing a cross-section of a multi-anvil Pt capsule of the hydrous experiment FD0853: the main occurring phases in this charge are in orange (Fe richer) ring and in light blue (Mg richer) ol. The upper part as in the previous picture, represent our buffer to minimize the incorporation of Fe^{3+}. The intensity color scale represents the distribution of Fe in the section.

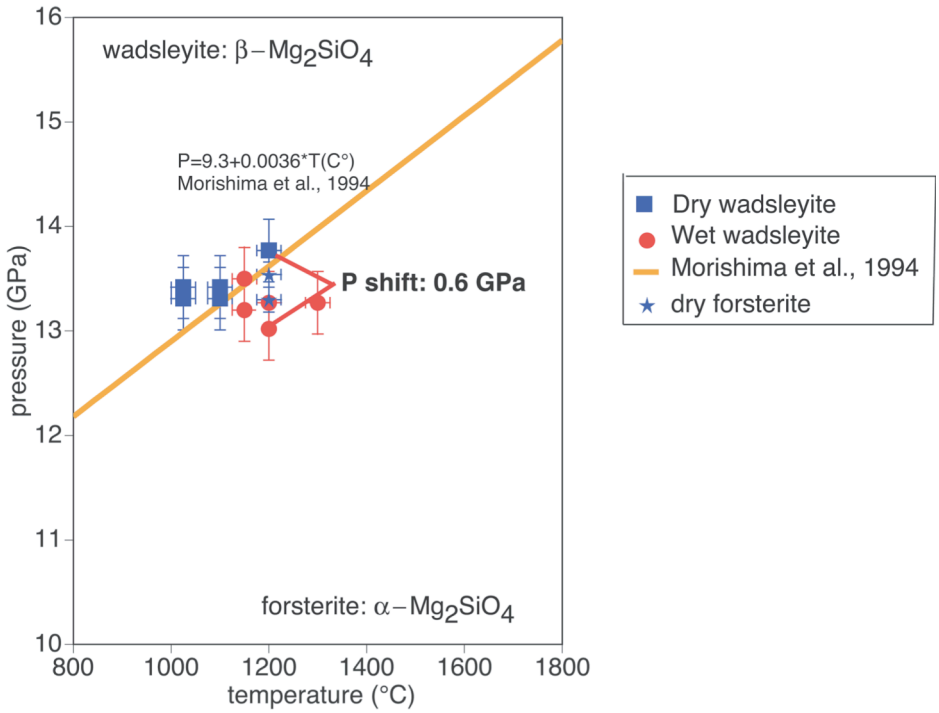

Fig. 3

Figure 3. P-T diagram showing the results of our experiments in the MgO-SiO_2-H_2O system: a shift of 0.6 GPa toward lower P values can be observed.

Results of the system MgO-SiO_2 ± H_2O are plotted in Figure 3 and listed in Table 1a. A systematic and replicate occurrence of hydrous wad in the stability field of olivine can be observed, thus provoking a shift of 0.6 GPa to lower P values at 1200°C.

To achieve a complete knowledge of the Earth upper mantle, Fe must be considered as additional element. We tried to keep the iron preferably in the divalent state as Fe^{2+} in order to exclusively link changes in the stability fields of the hydrous and anhydrous polymorphs to the presence of water. Figure 2b illustrates a cross-section of a Pt capsule of a Fe-bearing dry experiment where wad and ol coexist with the Fe-buffer at the bottom of the capsule. Wad is always Fe-richer than ol. In this experiment, the Fe-buffer contaminated a part of the experimental charge: the Fe-enriched area shows the presence of FeO (wüstite) even in the internal part of the buffer, indicating that our iron-wüstite buffer worked. Fe-fractionation data were collected far away from the Fe-enriched areas. The results of the experiments in the

system MgO-FeO-SiO_2 are plotted in Figure 4a. This P-x projection for 1200°C is based on the phase boundaries published by Agee (1998): the isothermally invariant line at 12 GPa indicates the coexistence of ol, wad and ring, e.g. the "triple point". The results of our dry experiments well reproduce within the experimental errors the phase boundaries proposed by Agee (1998), being thus a solid reference for our hydrous experiments.

Figure 2c represents a-cross section of a Fe-bearing wet-rotated run with coexisting ol and ring synthesized at 11 GPa and 1,200°C. Due to the rotation of the wet runs, our experimental charges were chemically homogeneous. In the experiment shown in Fig. 2c ring is always Fe-richer than ol, bearing a #Fe = 0.60 compared to ol with a #Fe = 0.21. Thus, Fe fractionates much more into ring than in wad, which is also expected from the phase diagrams. In wet runs carried out with the same constraints as other experiments but static, we observed not only a deviation in the #Fe (see Table 1b) but also a significant difference in the texture compared to rotated runs. Charges of static wet experiments always show chemically and mineralogical layered textures. Experiments in the system MgO-FeO-SiO_2-H_2O show different Fe fractionation among the coexisting phases compared to the dry runs (Table 1b) and allowed us to propose a new P-x projection at 1,200°C, shown in Figure 4b. The end-member ol-wad transition (x_{Mg} = 1) is plotted at 13.0 GPa based on our experiments system MgO-SiO_2-H_2O and the wad-ring transition (x_{Mg} = 1) at 21 GPa based on the results of Kawamoto (2004) who observed that the transition of wad to ring shifts in the presence of water to higher pressures. In replicate experiments, we could obtain coexisting hydrous ol-wad-ring, i.e. the triple point. A further experiment performed at 11 GPa and 1200°C, in the MgO-FeO-SiO_2-H_2O system showed ol-ring coexisting in paragenesis with enstatite. In total the stability field of hydrous wad expands in both directions, to lower (ol-wad loop) and higher (wad-ring loop) pressures, which can be linked to its higher water content compared to ol and ring.

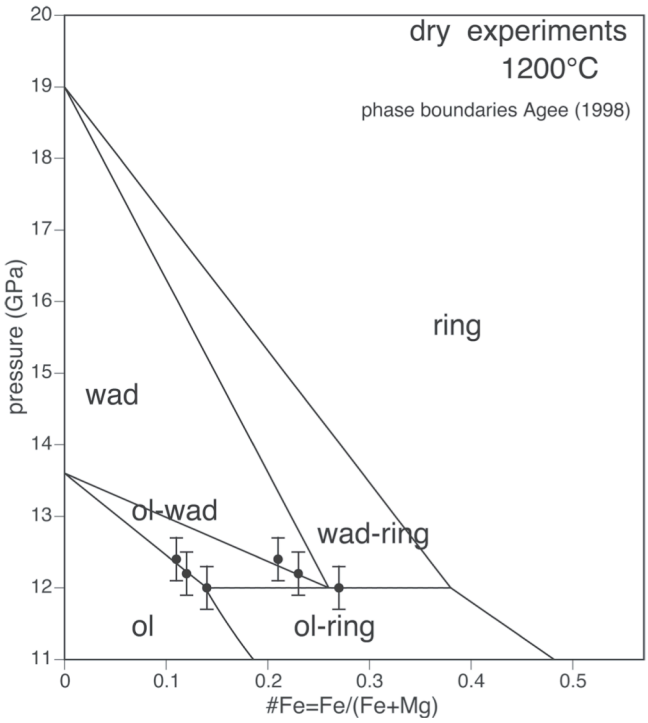

Fig. 4a

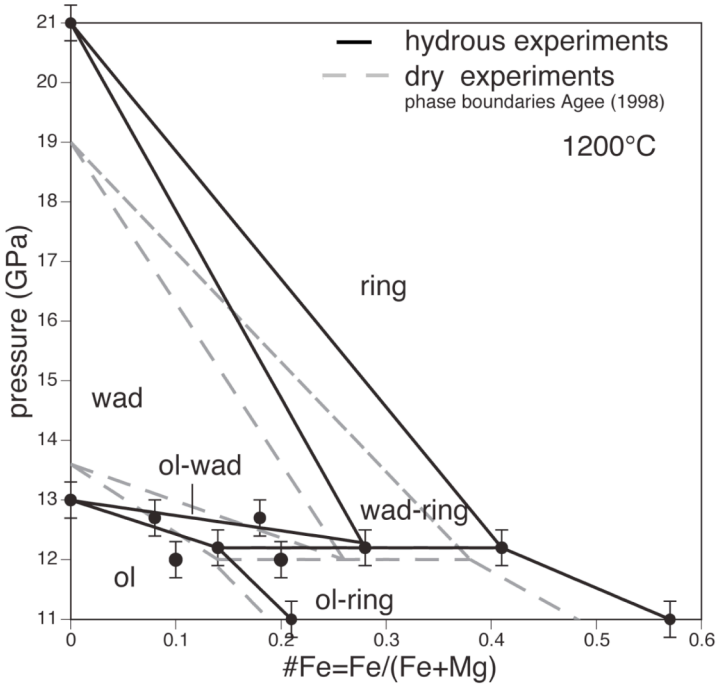

Fig. 4b

Figure 4 a) P-x projection at 1,200°C based on the phase boundaries suggested by Agee (1998) showing the results of our experiments at 12-12.4 GPa and 1,200°C in the system MgO-FeO-SiO_2. b) P-x projection at 1,200°C (solid lines schematic for clarity) constructed according to our results in the system MgO-FeO-SiO_2-H_2O between 11.0 and 12.7 GPa-1200°C and MgO-SiO_2-H_2O (13.0 GPa-1200°C) and considering the pressure uncertainty of 0.3 GPa. The Mg-end member wad-ring phase transition under hydrous condition was plotted at 21 GPa (Kawamoto, 2004). Compared to the dry system (*dashed gray lines*,) the regions where wad-ring and ring-ol coexist are broader in respect to the composition. The stability field of hydrous wad expands in both directions, to lower (ol-wad loop) and higher (wad-ring loop) pressures

The textures observed in the polished cross-sections of the capsules in the system MgO-FeO-SiO_2-H_2O shown in the backscattered pictures (Figure 5a, b, c) evidence symplectitic intergrowths, visible overall in the sections.

We observed in experiments FD0843 (anhydrous) and FD0844 (hydrous) the occurrence of an Al bearing phase, majorite (Figure 5e) coexisting with ol and wad, probably due to an impurity in the starting material. However, this is a minor phase and we determined the Fe-Mg partitioning data on ol and wad not in contact with majorite.

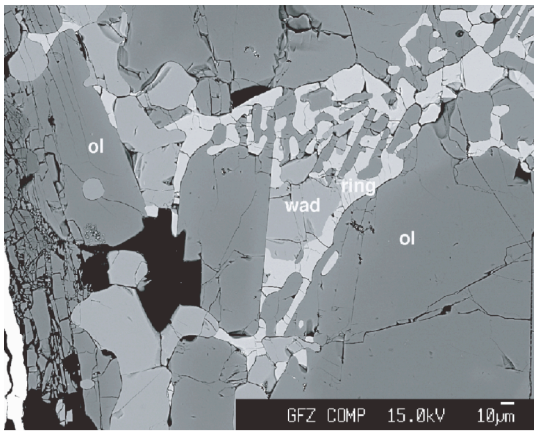

Fig. 5a

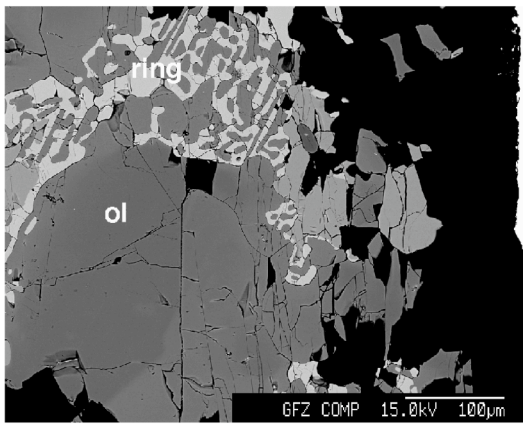

Fig. 5b

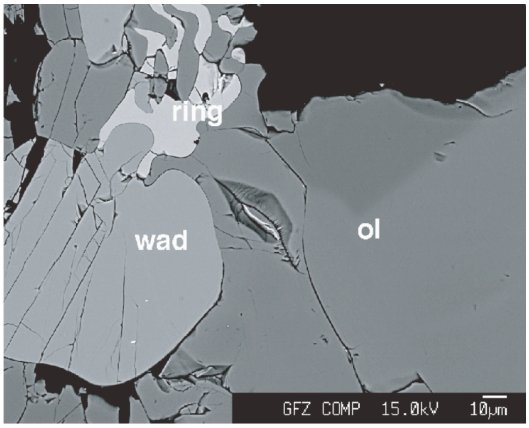

Fig. 5c

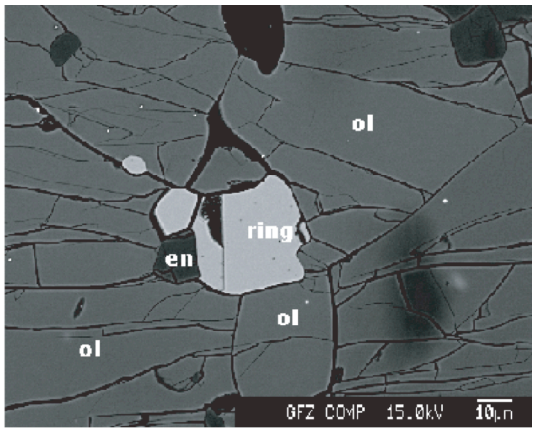

Fig. 5d

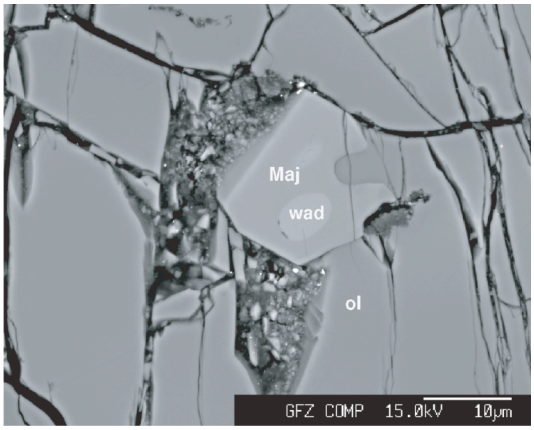

Fig. 5e

Figure 5 a) Electron microprobe backscattered picture showing coexisting ol, wad and ring (FD0833, 12.2 GPa and 1,200°C) the so-called triple point. The textures are also a strong sign of the equilibrium reached during the experiments. b) Detail of the texture of experiments FD0833: the three phases show a symplectitic texture.
c) Coexisting ol-wad-ring: on these crystals, we performed the SIMS measurements to quantify the water content.
d) Electron microprobe backscattered picture, where coexisting olivine ringwoodite in paragenensis with enstatite from the experiment FD0853 (11 GPa-1,200°C). e) Electron microprobe backscattered picture, showing majorite coexisting with olivine and wadsleyite, the experiment was performed at 12.4 (±0.3) GPa. Majorite occurred because of an impurity in the starting material used for the specific experiment FD0843

Water contents from different analytical methods

As FTIR spectroscopy has the highest detection limit for water in NAMs, crystals of hydrous and anhydrous runs, were analyzed in the OH stretching region. Although no water was added to the anhydrous runs it become obvious that especially wad was not really dry but contained about 20 wt ppm H_2O. The same was observed by Jacobsen et al. (2005). Interestingly, the spectra of this nearly dry wad clearly show that the asymmetric broad IR band occurring in the spectra of hydrous wad at about 3,300 cm^{-1} is indeed on overlap of three bands as proposed by Deon et al. (2009).

Crystals from hydrous runs of the pure Mg system contained according to the SIMS measurements 2,000 (±600) wt ppm H_2O for olivine (13.2 GPa-1,200°C), and as 8,000 (±1,000) wt ppm H_2O for wad (13.3 GPa-1,200°C). SIMS measurements in the system MgO-FeO-SiO_2-H_2O were carried out on one sample FD0833, synthesized at 12.2 GPa and 1,200°C on coexisting ol, wad and ring. Water was quantified for ol as 2,700 (±100) wt ppm H_2O, for wad as 10,000 (±1,000) wt ppm H_2O and for ring as 4,000 (±500) wt ppm H_2O. Partitioning coefficients were calculated as: $D^{water}_{wad/ol} \sim$ 3.7(5) and $D^{water}_{ring/ol} \sim$ 1.5(2) and $D^{water}_{wad/ring} \sim$ 2.5(5) (Table 2). Table 2. Water and Fe^{3+} quantifications.

Experiment	H_2O SIMS (wt ppm)	H_2O RAMAN (wt ppm)	H_2O FTIR (wt ppm)	H (pfu)	D^{water}	Fe^{3+} (pfu) EELS spectroscopy
FD0718	8,000 (±1,000)	-	-	0.13		-
FD0723	2,000 (±600)	-	-	0.03		-
FD0833	ol:2,700 (±100) wad:10,000 (±1,000) ring: 4,000 (±500)	wad:10,000 (±1,500)	-	0.04 0.16 0.06	$D^{water}_{wad/ol}$~3.7(5) $D^{water}_{ring/ol}$~1.5(2) $D^{water}_{wad/ring}$~2.5(5)	wad:0.070(20) ring:0.022(4)
FD0849	-	-	wad:12,000(±5,000)	0.19	-	-
FD0853	-	-	ol:3,800(±1,000) ring:3,300(±1,200)	0.06 0.05	$D^{water}_{ring/ol}$~0.87(33)	-

These values show that wad accommodate more water than the other two coexisting phases. Beside the SIMS quantifications, the results of the unpolarized RAMAN spectra collected on wad crystals of the same sample FD0833 provided a value, comparable to the SIMS data, of 10,000 (±1,500) wt ppm H_2O. Wad (FD0849) from a charge at lower P quantified with FTIR spectroscopy, gave as result 12,000 (±5000) wt ppm H_2O, within the uncertainty in good agreement with the quantifications obtained with SIMS and Raman spectroscopy. Unpolarized FTIR measurements averaged over several ol and ring crystals of experiment FD0853 provided water contents of 3,800 (±1000) wt ppm H_2O (ol) and 3300 (±1200) wt ppm H_2O for the coexisting ring. At lower P and higher Fe-concentrations, the partitioning coefficient between the two coexisting phases ol and ring is $D^{water}_{ring/ol}$~0.87(33).

TEM

EELS spectra (Figure 6) were collected in order to determine the Fe^{3+} content of the phases in the FIB foil obtained from the charge of experiment FD0833, on coexisting ol-wad-ring and on spinelloid in the foil of MA29 (see chapter 2.6). The Fe^{3+} concentration obtained by EELS for sample MA29 is in perfect agreement with that published by Koch-Müller et al. (2009). As for FD0833, Fe^{3+} fractionates preferentially in wad 0.070(20) pfu, while ring incorporates a minor quantity of 0.022(4). It was not possible to quantify the Fe^{3+} concentration for olivine because of the poor quality of the spectrum (Figure 6) due to the very low total Fe concentration. A longer acquisition time could have improved the spectrum; however, this may lead to an oxidation of the sample as Garvie and Busek (2004) observed. However, we estimate the Fe^{3+} content of ol to be close to zero, following previous studies (e.g. Frost and McCammon 2009).

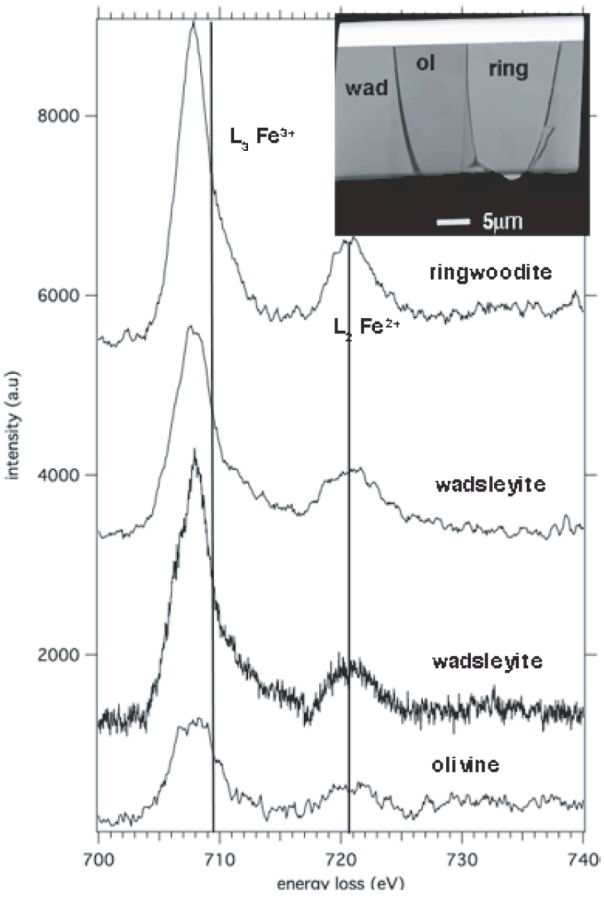

Fig. 6

Figure 6. Overview of the FIB foil obtained from the experiment FD0833 showing the three coexisting phases ol, wad and ring (triple point) that were obtained at 12.2 GPa and 1,200°C. b) EELS Fe $L_{2,3}$ edge spectra, the light asymmetry of the main peak indicate a small concentration of Fe^{3+}. Spectra were fitted following the method proposed by Van Aken (1998).

Discussion

Water concentration

System MgO-SiO_2-H_2O

At the P-T conditions typical of the Earth upper mantle, the parameter water solubility should be carefully considered because in the transition zone (TZ) the storage capacity, e.g. how much water can be incorporated by a mineral, can be only meant as equilibrium water content of a mineral that coexist with a hydrous melt or fluid. It is essential that this mineral species occur in a paragenesis that buffers the compositions of all coexisting phases so that the composition of a phase only depends on T and P. All our experiments were buffered with enstatite, and we had water in excess. Due to the sharpness of the phase transition water could not be quantified

on coexisting ol and wad. Nevertheless, we calculated a water partitioning coefficient as $D^{water}_{wad/ol} \sim$ 4 at 1200°C and 13.3 GPa on phases synthesized in different charges. This number is in good agreement with the D-value of 3.8 proposed by Demouchy et al. (2005) for similar conditions. As observed by Demouchy et al. (2005) partitioning coefficients $D^{water}_{wad/ol}$ decrease with increasing T, as the water solubility of wad decreases with increasing T.

System MgO-FeO-SiO_2-H_2O

The water content of Fe-bearing wad is slightly higher than that of the Mg-end member (Table 2). For coexisting ol-wad-ring we calculate the following water partitioning coefficients: $D^{water}_{wad/ol}$ ~ 3.7(5), $D^{water}_{ring/ol} \sim$ 1.5(2) (FD0833) and $D^{water}_{wad/ring} \sim$ 2.5(5). These coefficients suggest also in the Fe-bearing system a stronger fractionation of water in wad in comparison with the other two coexisting phases. To date Inoue et al. (2003) calculated the $D^{water}_{wad/ring}$ as 2.5, fairly similar to our value. However, in their conference abstract, the chemistry of their charges is not specified, thus their result is not suitable for comparison with our data. Chen et al. (2002) reported water concentration of 0.37 wt % for ol and 1.9 wt % for wad coexisting at 13 GPa and 1,200°C which results in $D^{water}_{wad/ol} \sim 5$. Their respective water contents were determined also by SIMS but using amphibole as standard, which most probably introduces a large uncertainty to the results due to matrix effects. Nevertheless, their results agree with ours so far that water also fractionates stronger into wadsleyite rather than in olivine. In the experiment, at lower pressure where we observed coexisting ol and ring the water partitioning coefficient was $D^{water}_{ring/ol} \sim 0.87(33)$. To the best of our knowledge, this is the first partitioning coefficient for coexisting ol and ring under these conditions.

Evidence of equilibrium

The long run duration (>24 hours) and the results of replicate runs in the hydrous and anhydrous MgO-FeO-SiO_2 system certifies that we reached equilibrium during our

experiments. Further proofs of equilibrium are the textures shown in the backscattered pictures. Figure 5a, b, c evidence symplectitic textures, visible overall in the section. One can distinguish large parts of olivine with intergrowths of wad and ring. We interpret these textures with metastable ol-growth during the 30-min heating period and exsolution of the stable phase assembly ol-wad-ring when P-T of the experiments was reached and maintained for more than 24 hours. Kerschofer et al. (1998) performed kinetic experiments where they brought ol into the stability field of ring and analyzed the changes in the phase assembly and texture after a certain time. They always observed thin lenses of ol within the ring grains. They interpret this as an indication of metastable occurrence of the ol in the much harder grains of the high pressure polymorph ring. Our textures show no olivine occurring as relict in our ringwoodite - we even observe the opposite as olivine occurs as well-formed crystal and is the major occurring phases throughout the capsule. Another evidence of equilibrium is the texture in experiment FD0853, where we observe coexisting ol and ring. The dominant occurring phase is Fe-bearing ol and the occurrence of ring is limited to small parts of the capsule, which is to be expected from the composition of the starting material and the lever rule.

Influence of water on the phase stability

System MgO-$SiO_2 \pm H_2O$

Our hydrous experiments showing the systematic occurrence of hydrous wad in the stability field of olivine evidenced that the phase boundary between ol and wad, is shifted by 0.6 GPa (~ 18 km) to lower pressure compared to the dry system at 1200°C. Previously Chen et al. (2002) observed no relevant difference in the ol-wad phase boundary between hydrous and anhydrous conditions. Frost and Dolejs (2007) disagreed with the results of Chen et al. (2002), as they observed at 1,200°C a shift of 1.0 GPa to lower pressure under hydrous conditions compared to anhydrous conditions. Unfortunately, Frost and Dolejs (2007) did not

determine the water content of their phases. But the amount of water incorporated by the phases characterizing the transition zone determines the shift of the phase boundary. The preferential partitioning of water in wad and its statistically distribution in the structure (e.g. Deon et al. 2009) stabilize wad to lower pressure through the configurational entropy. Thus, our observation is theoretically expected.

Wood (1995) was the first who calculated the effect of water on the phase boundaries; he calculated that as little as 500 ppm water incorporated in ol and assuming ten times more water in wad displaces the phase boundary of 0.6 GPa to lower pressure. Although ol and wad contain a different amount of water in our experiments, the shift that we observed experimentally agrees with the displacement to lower P calculated by Wood. On the base of new crystal chemical data, Frost and Dolejs (2007) revised the thermodynamic model of Wood and provide Eq. 1, where the effect of H_2O on the 410-km discontinuity in the MgO-SiO_2-H_2O system can be calculated as shift ΔP.

$$\Delta P \Delta V = RT \ln\left[\left(\frac{0.5 - V_{Mg}}{0.5}\right)^{0.5}\right]_{wad} - RT \ln\left[\left(1 - V_{Mg}\right)\right]_{ol} \qquad (1)$$

where the T is expressed in K and P in GPa. $V_{Mg}=\frac{n(OH)}{2}$ requires the OH concentration in wad and ol based on the fact that in both minerals 2 OH are incorporated via one Mg vacancy; ΔV is the volume change of reaction, approximately -2,200 J/GPa (Frost and Dolejs 2007).

The expression for the configurational entropy for wad in Eq. 1 is based on the observation that only one half of the available M3 sites are protonated (Smyth et al. 1987). Deon et al. (2009) confirmed this incorporation mechanism. They specify that the hydration of wad occurs along the O1•••O4 and/or O3•••O4 edges of a vacant M3 octahedron. H is bounded either on two O1, two O3, or on one O1 and one O3 sites of a vacant M3 site. As for ol, Frost and Dolejs (2007) assume in their thermodynamic model that vacancies related to OH incorporation occurs on all M1 sites leading to the expression for the configurational entropy

given in equation 1. Frost and Dolejs (2007) took literature data for the maximum solubility of water in wad and ol as 2.5 wt% and 0.8 wt%, respectively, and calculated a shift of 1 GPa to lower pressures at a temperature of 1,200°C. Because we were not able to produce coexisting ol and wad in our experiments in the system $MgO\text{-}SiO_2\text{-}H_2O$, we assume that the water partitioning is similar to that in the Fe-bearing system and calculated the pressure shift using the water contents determined with SIMS of the coexisting wad and ol in experiment FD0833. With these values, we obtained a shift of the ol-wad phase boundary of 0.4 GPa to lower pressure - very close to that what we observe experimentally.

System $MgO\text{-}FeO\text{-}SiO_2 \pm H_2O$

$K_{wad/ol}^{Fe/Mg} = \left[(Fe/Mg)_{wad} / (Fe/Mg)_{ol} \right]$ of dry runs performed in the P interval 12 - 12.4 GPa and the same T shows values ranging between 2.15-2.86 (Table 1b). Our Fe-Mg partitioning coefficients between ol and wad are similar to the values calculated by Chen et al. (2002) in dry experiments (2-2.6). Other data, e.g. Katsura et al. (2004), scatter too much to be compared with our data most likely due to a shorter run duration compared to our study. Hydrous experiments of this study performed in the same P range show $K_{wad/ol}^{Fe/Mg}$ values of 2.23-2.60. Thus, water does not have a considerable influence on these values. Experiments of Chen et al. (2002) were performed exclusively in the system $(Mg_{0.91}Fe_{0.09})_2SiO_4$ and cannot be compared to our study as the initial bulk composition strongly influences the values of $K^{Fe/Mg}$.

According to Agee (1998), the triple point where ol, wad and ring coexist occurs under dry conditions at 12 GPa and 1,200°C. In our hydrous experiments, we observe the triple point at 12.2 GPa and 1200°C. However, we would not speculate that water affects the P where the triple point occurs as the uncertainty in pressure of our experiments is about ± 0.3 GPa. This uncertainty is reflected in the results of experiment FD0849 performed at 12.0 GPa but

showing coexisting ol and wad with compositions, which must correspond to a higher pressure than the triple point.

To provide a real description of the effect of H_2O on the Earth upper mantle, the results of the MgO-SiO_2-H_2O and MgO-FeO-SiO_2-H_2O systems must be combined and we propose a new phase diagram (Figure 4b). Water, according to our results, strongly modifies the phase diagram. We assume that the very small amounts of Fe^{3+} incorporated in wad, ring and ol in this study do not influence the phase boundaries of the MgO-FeO-SiO_2-H_2O system. Therefore, we plot in the diagrams only the #Fe = Fe/ (Fe + Mg), where Fe_{tot} is calculated as Fe^{2+}.

In the new hydrous phase diagram, the data indicate an expansion of the wad stability field toward lower and higher pressure. For a bulk composition of $x_{Fe} = 0.1$, which represents the average composition of the Earth upper mantle, our data indicate only a slight difference in the width of the loop of the two-phase field ol-wad under wet conditions compared to dry conditions, i.e. no broadening with respect to composition but a shift to lower pressure. There could be a slight decrease of the pressure width of the loop as observed by Chen et al. (2002) but due to the uncertainties in pressure of ± 0.3 GPa, such a small difference cannot be verified. Contrary to Chen et al. (2002), we observe under wet conditions no shift of the loop toward lower iron contents. Such a shift can be related to Fe^{3+} incorporation: Frost and McCammon (2009) showed that under oxidizing conditions both boundaries of the ol-wad loop shift to lower iron contents. Opposite to Chen et al. (2002), we performed our experiments under reducing conditions and we checked the low Fe^{3+} incorporation. Therefore, we link the observation of Chen et al. (2002) to the presence of both water and Fe^{3+} in their run products. Thus, the seismic observations by van der Meijde et al. (2003) that the 410-km has a varying thickness, between 390-440 Km, across the Earth may be related to both variable Fe^{3+} and water incorporation.

For bulk compositions of $x_{Fe} > 0.2$, i.e. in regions where wad-ring and ol-ring coexist, we observe a broadening and a shift of the loops to higher iron contents. This is a very interesting

and unexpected result and should be investigated in further studies. One explanation for this observation could be that with increasing Fe content ringwoodite incorporates under these conditions more water and thus Fe-rich ringwoodite would be stabilized through the increase of the configurational entropy (see section influence of water on the phase stability).

Conclusion

The presence of water induces a significant effect on the stability fields of $(Mg,Fe)_2SiO_4$ polymorphs in both the MgO-SiO_2-H_2O and the MgO-FeO-SiO_2-H_2O system. Incorporation of 0.8 wt% water in Mg-wad and 0.2 wt% in Mg-ol displaces the ol-wad phase boundary, 0.6 GPa to lower P, which agrees within the uncertainties with the value (1 GPa) proposed by Frost and Dolejs (2007). In the MgO-FeO-SiO_2-H_2O system, water seems to have only little effect on the ol-wad loop - it is only shifted to lower pressures. We found neither a broadening nor a shift of the loop to lower Fe-contents as previously Chen et al. (2002) observed. Combining our results with the results from the more oxidized experiments of Frost and McCammon (2009), we propose that the shift to lower Fe concentration found by Chen et al. (2002) is due to incorporation of Fe^{3+} rather than OH. A slight decrease of the width of the loop might occur. However, in more Fe-rich compositions, the presence of water broadens the loops where wad-ring and ol-ring coexist. In total the stability field of hydrous wad expands in both directions, to lower (ol-wad loop) and higher (wad-ring loop) pressures.

Acknowledgements

We thank Reiner Schulz for his important help and technical support during the multi-anvil press experiments and Julia Pohlenz. We are also very grateful to Dr. Michael Wiedenbeck for the precious help during the SIMS measurements. Further, we greatly appreciated the help of Oona Appelt (EMPA), Ilona Schäpan (SIMS) and the precious work of Anja Schreiber who prepared the FIB foils that were analyzed at TEM. We also thank Hans-Peter Nabein for his

help in collecting the powder XRD-diffraction pattern. Last but not leas, we are very grateful to Stefan Gehrmann and Gerhard Berger who prepared the samples for the EMPA and SIMS. The quality of this manuscript was improved, thanks to the suggestion and comments by an anonymous reviewer and of the editor Jochen Hoefs. This study was supported by a grant from Deutsche Forschungsgemeinschaft within the priority program SPP1236 under grant KO1260/7-1.

References

Agee CB (1998) Phase transformations and seismic structure in the upper mantle and transition zone. *In*: Ultrahigh-pressure mineralogy: Physics and chemistry of the Earth's Deep Interior. Mineralogical Society of America

Armstrong JT (1995) CITZAF A package of correction programs for the quantitative electron microbeam X-ray analysis of thick polished materials, thin films, and particles. Microbeam Analysis 4: 7–200

Chen J, Inoue T, Yurimoto H, Weidner JD (2002) Effect on olivine-wadsleyite phase boundary in the $(Mg,Fe)_2SiO_4$ system. Geoph Res Lett 29 (18): 1875

Demouchy S, Deloule E, Frost DJ, Keppler H (2005) Temperature and pressure dependence of water solubility in iron – free wad. Am Mineral 81: 1084 – 1091

Deon F, Koch-Müller M, Rhede D, Gottschalk M, Wirth R, Thomas S-M (2009) Location and quantification of hydroxyl in wadsleyite: new insights. Am Mineral 95: 312-322

Dziewonski AM, Anderson DL (1981) Preliminary reference Earth model. Phys Earth Planet Inter 25: 297-356

Frost DJ, Dolejs D (2007) Experimental determination of the effect of H_2O on the 410-km discontinuity. Earth Planet Sci Lett 256: 182-195

Frost DJ, McCammon C (2009) The effect of oxygen fugacity on the olivine to wadsleyite transformation: implications for a remote sensing of mantle redox state at the 410-km seismic discontinuity. Am Mineral 94: 872-882

Garvie LAJ, Buseck PR (2004) Unoccupied states of pyrite probed by energy-loss spectroscopy (EELS). Am Mineral 89: 485-491

Inoue T, Yurimoto H, Kudoh Y (1995) Hydrous modified spinel, $Mg_{1.75}SiH_{0.5}O_4$: a new reservoir in the mantle transition region. Geophys Res Lett 22: 117-120

Inoue T, Wada T, Sasaki R, Irifune T, Yurimoto H (2003) Partitioning of H_2O on high pressure phase transformation of olivine. American Geophysical Union, Fall Meeting (abstract #V42A-0318

Katsura T, Ito E (1989) The system Mg_2SiO_4-Fe_2SiO_4 at high pressures and temperatures: precise determination of stabilities of olivine, modified spinel, and spinel. J Geophy Res 97: 15663-15670

Katsura T, Yamada H, Nishikawa O, Song M, Kubo A, Shinmei T, Yokoshi S, Aizawa Y, Yoshino T, Walter MJ, Ito E (2004) Olivine-wadsleyite transition in the system $(Mg,Fe)_2SiO_4$. J Geoph Res, 109: B02209

Kawamoto T (2004) Hydrous phase stability and partial melt chemistry of H_2O-saturated KLB-1 peridotite up to the uppermost lower mantle conditions. Phys Earth Planet Inter 143-144: 387-395

Keppler H, Bolfan-Casanova N (2006) Thermodynamics of water solubility and partitioning. In: Keppler H, Smyth J.R, (eds) Water in nominally anhydrous minerals, vol. 62 American Mineralogical Society. Geochemical Society, Chantilly, pp. 193-230.

Kerschhofer L, Dupas C, Ming L, Sharp TG, Durham WB, Rubie D (1998) Polymorphic transformations between olivine, wadsleyite and ringwoodite: mechanisms of intracrystalline nucleation and the role of elastic strain. Min Mag 62(5): 617-638

Koch-Müller M, Rhede D (2010) IR absorption coefficients for water in nominally anhydrous high-pressure minerals. Am Mineral 95: 770-775

Koch-Müller M, Matsyuk SS, Rhede D, Wirth R, Khisina N (2006) Hydroxyl in mantle olivine xenocrysts from Udachnaya kimberlite pipe. Phys Chem Min 33: 276-287

Koch-Müller M, Rhede D, Schulz R, Wirth R (2009) Breakdown of hydrous ringwoodite to pyroxene and spinelloid at high P and T and oxidizing conditions. Phys Chem Min 36: 329-341.

Kohlstedt DL, Keppler H, Rubie DC (1996) Solubility of water in the α, β and γ phases of (Mg, $Fe)_2SiO_4$. Contr Min Petr 123: 345 – 357

Lauterbach S, McCammon, CA, Van Aken P, Langenhorst, F Seifert, F (2000) Mössbauer and ELNES spectroscopy of (Mg, Fe)(Al,Si)O_3 perovskite: a highly oxidized component of the lower mantle. Contrib Mineral Petrol 138: 17-26

Libowitzky E, Rossman G R (1997) An IR absorption calibration for water in minerals. Am Mineral 82: 1111-1115

Maldener J, Hösch A, Langer K, Rauch F (2003) Hydrogen in some natural garnets studied by nuclear reaction analysis and vibrational spectroscopy. Phys Chem Min 30: 337-344

Morishima H, Kato T, Suto M, Ohtani E, Urakawa S, Utsumi W, Shimomura O, Kikegawa T. (1994) The phase boundary between α-and β-Mg_2SiO_4 determined by in situ X-ray observation. Science 26: 1202-1203

Mosenfelder JD, Deligne NI, Asimow PD, Rossman GR (2006) Hydrogen incorporation in olivine from 2-12 GPa. Am Mineral 91: 285-294

Paterson MS (1982) The determination of hydroxyl by infrared absorption in quartz, silicate glasses and similar materials. Bull de Minéral 105: 20–29

Ringwood AE (1975) Composition and petrology of the Earth´s mantle. McGraw Hill, New York

Ross NL (1997) Optical Absorption Spectra of Transition Zone Minerals and Implications for Radiative Heat Transport. Phys Chem Earth 22: 113-118

Rossman GR (2006) Analytical methods for measuring water in nominally anhydrous minerals. In H. Keppler, and J.R. Smyth, Eds. Water in Nominally Anhydrous Minerals, vol. 62. American Mineralogical Society. Geochemical Society, Chantilly (Vir.) pp. 1-28

Rost R, Weber M (2002) The upper mantle transition zone discontinuities in the Pacific as determined by short period term array data. Earth Planet Sci Lett 204: 347-361

Schmidt MW, Ulmer P (2004) A rocking multi-anvil: elimination of chemical segregation in fluid-saturated high-pressure experiments. Geoch Cosmoch Acta 68: 1889-1899

Smyth JR (1987) β-Mg_2SiO_4: A potential host for water in mantle? Am Mineral 72: 1051-1055

Smyth JR (2006) Hydrogen in High Pressure Silicate and Oxide Mineral Structures. Rev Miner Geochem 62: 85-115

Thomas S-M, Thomas R, Davidson P, Reichart P, Koch-Müller M, Dollinger G (2008) Application of Raman spectroscopy to quantify trace water concentrations in glasses and garnets. Am Mineral 93: 1550-1557

Thomas S-M, Koch-Müller M, Reichart P, Rhede D, Thomas R, Wirth R, Matsyuk S (2009) IR calibrations for water determination in olivine, r-GeO_2 and SiO_2 polymorphs. Phys Chem Min 36: 489-509

Van Aken PA, Liebscher B, Styrsa VJ (1998) Quantitative determination of iron oxidation states in minerals using Fe L 2,3 -edge electron energy-loss near-edge structure spectroscopy. Phys Chem Min 25: 323-327

van der Meijde M, van der Lee S, Giardini D (2003) Seismic evidence for water deep in Earth´s upper mantle. Science 300: 1156-1558

Walker D (1991) Lubrication, gasketing, and precision in multi-anvil experiments. Am Mineral 76: 1092-1100

Wirth R (2004) A novel technology for advanced application of micro- and nanoanalysis in geosciences and applied mineralogy. E J Min 16 6: 863-876

Wood BJ (1995) The effect of H_2O on the 410-km seismic discontinuity. Science 268: 74-76

Yamazaki A, Hirahara K (1994) The thickness of the upper mantle discontinuities as inferred from short-period J-Array data. Geoph Res Lett 21: 1811-18